RSC Advances

ROYAL SOCIETY OF CHEMISTRY

www.rsc.org/advances

RSC Advances

RSCPublishing

ARTICLE

Binder-free hydrogenated NiO-CoO hybrid electrodes for high performance supercapacitors

Cite this: DOI: 10.1039/x0xx00000x

Received 00th January 2012,
Accepted 00th January 2012

DOI: 10.1039/x0xx00000x

www.rsc.org/

Mingyang Yang,[ab] Fucong Lv,[b] Zhenyu Wang,[ab] Yiqiu Xiong,[a] Minchan Li,[ab] Wenxi Wang,[b] Lihua Zhang,[b] Sisi Wu,[b] Hongtao Liu,[a] Yingying Gu,[*a] and Zhouguang Lu[*b]

Binder-free NiO-CoO hybrid electrodes were directly grown on the nickel foam by electrodeposition and subsequently annealing in 5% H_2/ 95% N_2 gas at 300℃. Crystal structure, elemental analysis, surface morphology and chemical compositions of the composites were characterized by X-ray diffraction (XRD), X-ray photoelectron spectroscopy (XPS), scanning electron microscopy (SEM) and transmission electron microscopy (TEM) equipped with an energy dispersive X-ray analysis system. The hydrogenated NiO-CoO hybrid electrodes were evaluated as electrode for supercapacitors which demonstrated promising electrochemical performance with high specific capacitance, excellent rate capability, and stable cycling.

1. Introduction

Supercapacitors attracted great recent research interest because of their ultrafast charge/discharge capability, extremely long cycle life, high power density, and remarkable safety. Supercapacitors have been successfully applied in the fields of digital cameras, mobile phones, electrical tools and pulse laser technology.[1-4] Transition metal oxides (TMOs) such as RuO_2, MnO_x, SnO_2, V_2O_5, Fe_2O_3/Fe_3O_4, NiO and Co_3O_4/CoO are widely considered as pseudo-capacitive electrodes for supercapacitors in value of their environmental benignity, low cost, and high capacitance.[5-13] However, in comparison with the carbon based electrode materials, transition metal oxides have relatively poor cycle life because of slow ion diffusion rates, poor electron conductivity and volume variation upon electrochemical reaction which are largely inhibiting their practical applications in supercapacitors particularly considered for EVs.

Recently, there are two main methods to enhance the electron conductivity of the pseudocapacitive electrode materials. On the one hand, binary transition metal oxides have been reported to demonstrate better performance than single-component counterpart due to their feasible oxidation states and high electrical conductivity, such as $NiCo_2O_4$,[14-16] $MnCo_2O_4$,[17, 18] $CoMn_2O_4$,[19] $ZnCo_2O_4$,[20, 21] $NiMoO_4$,[22, 23] and $CoMoO_4$.[24, 25] On the other hand, binder-free supercapacitive electrodes directly grown on three-dimensional conductive substrates such as nickel foam, carbon nanotube arrays or porous metallic films have attracted great attention because it can reinforce the interfacial contact between the current collector and active materials and thus enhance the ion and electron transport, leading to much improved electrochemical performance. Additionally, much attention has been focused on improving the specific capacitance of supercapacitors by exploring novel materials with the rational design of multi-component combination, which can provide the synergistic effect of all individual constituents, as well as controllable 3D hierarchical heterostructures, which can provide efficient and rapid pathways for ion and electron transport, not only at their surfaces, but throughout the bulk chemical distributions.[26, 27] Fan et al. reported Co_3O_4/NiO core/shell nanowire arrays on a Ni foam substrate by hydrothermal and chemical bath deposition methods as an electrode material, which showed a specific capacitance of 853 F g^{-1} at 2 A g^{-1} and good cycling stability.[28] Also, CoO@$Ni(OH)_2$ hybrid nanostructures on Ni foam have been fabricated by the electrodeposition process for pseudocapacitors, which have a high area capacitance up to 11.5 F cm^{-2}.[29] Tong et al. reported Co_3O_4/$Ni(OH)_2$ composite mesoporous nanosheets on Ti substrates via an electrochemical deposition route, which showed a high specific capacitance of 1144 F g^{-1} and long-term cyclability.[30] Although better electrochemical properties have been achieved, the fabrication processes involving substrate materials and deposition growth are complicated, time-consuming, and have low repeatability, and particularly, the as synthesized products have a low yield, thus hindering their wide commercial applications in energy storage system. It is thus highly desirable to design hybrid architectures with excellent electrochemical properties and to develop a facile, environmentally friendly, low-cost, and large-scale synthetic method for supercapacitor applications.

In this paper, we developed a simple method to prepare NiO-CoO hybrid nanosheets directly grown on nickel foam for high-performance supercapacitors. The facile fabrication procedure is schematically illustrated in Fig. 1. Firstly, the Ni-Co layered double hydroxides (LDH) precursor was firstly prepared by a simple electrodeposition method. Then, the precursor was annealed in a reductive conditions provided by a mixed gas of 5% H_2 /95% N_2 at 300℃ for 2h. The hydrogenated Ni@NiO-CoO hybrid nanosheets exhibited greatly enhanced electrochemical performance, in terms of high specific capacitance, remarkable rate performance, and outstanding cycling stability, compared to the conventional

Ni@$NiCo_2O_4$ nanosheets obtained by annealing the precursor in pure N_2 gas.

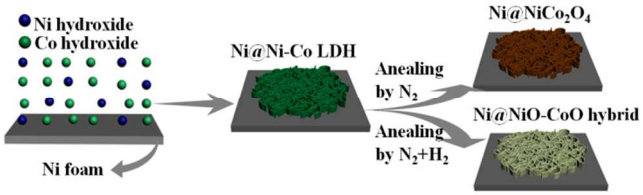

Fig. 1 Schematic illustration of the fabrication process of the hydrogenated Ni@NiO-CoO hybrid nanosheets and the conventional Ni@$NiCo_2O_4$ nanosheets.

2. Experimental section

2.1 Preparation of Ni-Co hydroxides on nickel foam

All the chemicals used were of analytical grade and used without further purification. The nickel nitrate hexahydrate ($Ni(NO_3)_2{\cdot}6H_2O$), cobalt nitrate hexahydrate ($Co(NO_3)_2{\cdot}6H_2O$), hydrochloric acid (HCl), potassium hydroxide (KOH) and absolute ethanol were purchased from Sinopharm Chemical Reagent Co., Ltd.. Deionized water was used. The electrochemical deposition of Ni-Co hydroxide precursor was carried out in a three-electrode cell at a constant current of -1 mA cm^{-2}. The working electrode was a piece of nickel foam (1 cm×1 cm) which was treated with 3 M HCl for 10 min to remove the surface oxide layer and then washed thoroughly with deionized water before the electro-deposition. Pt plate and SCE (saturated calomel electrode) was used as the counter and reference electrode, respectively. The electro-deposition time during the constant current deposition was fixed at 10 minutes.

2.2 Synthesis of Ni@NiO-CoO hybrid nanosheets and Ni@ $NiCo_2O_4$ nanosheets

In order to obtain Ni@NiO-CoO hybrid nanostructures, the as-prepared Ni-Co hydroxide precursor was transferred into a tube furnace, and calcined at 300℃ for 2 hours under a flowing N_2 and H_2 (5 at%) mixed gas. In the H_2 reducing process, the Ni-Co hydroxide precursor was dehydrated and reduced to a homogeneous nanocomposite of NiO and CoO hybrid phase.The conventional Ni@ $NiCo_2O_4$ was obtained by the similar method by using highly pure N_2 gas instead of H_2/N_2.

2.2 Materials Characterizations

XRD data were collected using a Rigaku D/MAX 2400 diffractometer (Japan) with Cu Kα radiation (k=1.5418Å) operating at 40.0 kV, 60.0 mA. Field emission scanning electron microscopy (FESEM) measurement was conducted on a Hitachi S-4800 scanning electron microscope. HRTEM image and energy dispersive X-ray spectroscopy (EDX) measurements were obtained on a transmission electron microscopy (FEI Tecnai G2 F30). X-ray photoelectron spectroscopy (ESCALAB 250 Xi, Thermo Fisher) measurements were conducted to investigate the different valence state of Ni and Co for Ni@NiO-CoO hybrid and the Ni@ $NiCo_2O_4$.

2.3 Electrochemical characterization

Electrochemical performance was evaluated by using a three-electrode configuration and employing 6 M KOH as electrolyte, Pt plate as counter electrode, and Hg/HgO as reference electrode. Cyclic voltammetry (CV) was performed on a CHI660E electrochemical workstation (Chenhua, Shanghai). The galvanostatic charge/discharge data were collected on a Neware (CT-4008) cycler.

3. Results and discussion

3.1 Structure and Morphology

Fig. 2a shows the XRD patterns of Co–Ni LDHs, hydrogenated NiO-CoO hybrid and $NiCo_2O_4$ separately grown on nickel foams. The peaks marked with grey circle originated from the nickel foam. Before calcination, as shown in Fig. 2a (blue curve), the four main broad peaks at 2θ values of 11.4, 22.8, 34.0 and 59.6 can be indexed to the typical Co–Ni LDHs consisting of α-$Ni(OH)_2$ and α-$Co(OH)_2$.[31] After calcination in N_2 gas, the Co–Ni LDHs were completely converted into $NiCo_2O_4$ as revealed in Figure 2a (red curve). Except for the three typical peaks originating from the Ni foam, other six well defined diffraction peaks are observed at 2θ values of 18.9°, 31.1°, 36.6°, 59.1°, 64.9° and 68.3°. All of these peaks can be well assigned to the (111), (220), (311), (511), (440) and (531) plane reflections of the spinel $NiCo_2O_4$ crystalline structure (JCPDF file no. 20-0781), with the standard peaks indicated by the red rhombus.[15] The black curve in Fig. 2a shows the sample obtained by annealing the precursor in a H_2/N_2 mixed gas with 5% H_2. The four weak peaks appearing at the 2θ value of 37.2°, 43.3° and 62.9° are indexed to the (111), (200) and (220) planes of the CoO phase (JCPDS Card No. 48-1719) and NiO phase (JCPDS Card No. 47–1049).[13, 32-35] To obtain a more detailed elemental composition and the oxidation state change of Ni@$NiCo_2O_4$ and Ni@NiO-CoO hybrid nanostructures, XPS tests was performed. The complete surveys of Ni@$NiCo_2O_4$ and Ni@ NiO-CoO hybrid in Fig. 2b reveals the existence of Ni 2p and Co 2p. The high resolution Ni 2p 1/2 and Co 2p 3/2 XPS spectra of the $NiCo_2O_4$ was shown in Fig. 2c and d, respectively. By using a Gaussian fitting method, the Ni 2p emission spectrum (Fig. 2 c) was best fitted with two spin-orbit doublets, characteristic of Ni^{2+} and Ni^{3+}, and one shakeup satellite (indicated as "Sat.").[36] The Co 2p (Fig. 2d) was also fitted with two spin-orbit doublets, characteristic of Co^{2+} and Co^{3+}, and two shakeup satellites. These XPS results clearly demonstrate that the surface of the prepared $NiCo_2O_4$ has a mixed composition containing Co^{2+}, Co^{3+}, Ni^{2+} and Ni^{3+}. Unfortunately, the absolute binding energy of the 2p3/2 peak is not always very helpful in identifying the cobalt chemical environment in the CoO and $NiCo_2O_4$, since relatively small shifts are reported to accompany oxidation of Co^{2+} to Co^{3+}.[37-41] In the Fig. 2e and 2f, the nickel 2p and cobalt 2p binding energies and peak shape of the NiO-CoO are very similar to the $NiCo_2O_4$ as shown in Fig. 2c and d and it is hard to identify the valence state change of Co^{2+} converting to Co^{3+}. However, the 2p3/2 to 2p1/2 separation and satellite structure has elements that are useful in characterizing the cobalt chemical environment. Octahedral Co^{2+} cations, as found in CoO for example, have a very intense, characteristic satellite at ~787 eV, the approximate position of which is indicated by the purple arrow of Fig. 2f, multiplet splitting causes extensive broadening in the CoO 2p spectrum, so that despite the fact that the monoxide has a single type of cobalt (octahedral Co^{2+}), its 2p3/2 spectrum is actually broader than that of $NiCo_2O_4$, the latter phenomenon is indication of two types of cobalt (tetrahedral Co^{2+} and octahedral Co^{3+}) contributing to this spectral region.[41] The XPS results are evidenced as the reduzate of NiO-CoO by annealing the Ni-Co hydroxide in H_2 gas.

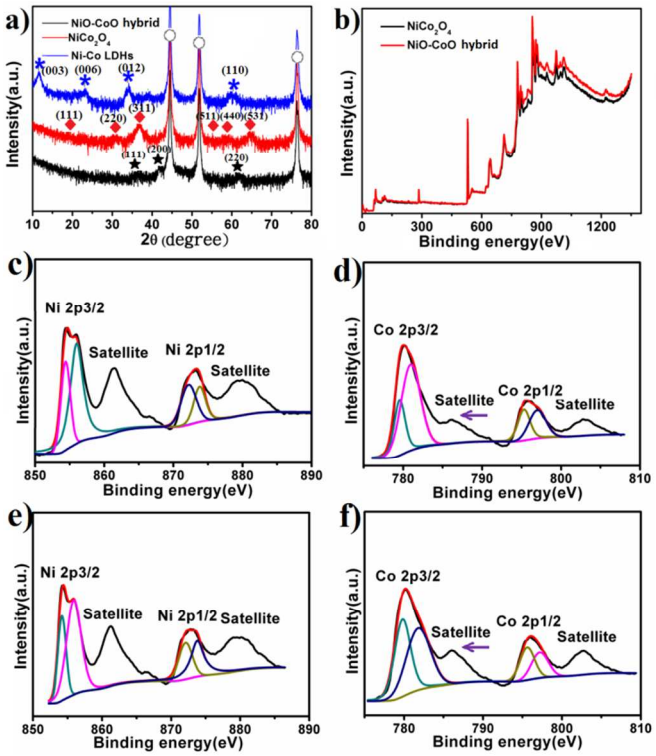

Fig. 2 (a) XRD patterns of the as-prepared $NiCo_2O_4$ (back), Ni@Ni-Co oxide(red), (b) XPS spectra of survey spectrum, Ni 2p (c), Co 2p (d) in the as-prepared $NiCo_2O_4$ (c and d), Ni@ NiO-CoO hybrid (e and f) .

Fig. 3a shows a representative low-magnification field emission scanning electron microscopy (FESEM) image of the nickel foam substrate. Clearly, a 3D grid structure with hierarchical macro-porosity can still be found as that in the pristine Ni foam. Fig. 3b indicates that the precursor obtained by the electrodeposition is comprised of nanosheets. After annealing for 2 hours, the Ni@$NiCo_2O_4$ (Fig. 3c) and Ni@NiO-CoO hybrid (Fig. 3d) nanostructures are achieved separately in the N_2 gas and 5% H_2/95% N_2 mixed gas and their surface morphology are almost the same to the precursor. Therefore, the architecture of nanosheets forming macroporosity was well preserved during the fast annealing step with the conversion of Ni-Co hydroxide to $NiCo_2O_4$ and NiO-CoO hybrid.

High resolution transmission electron microscopy (HRTEM) measurements were carried out to further investigate the different structures of the as-synthesized $NiCo_2O_4$ and NiO-CoO hybrid nanosheets. Fig. 4a~d show the high resolution TEM images and the corresponding SAED patterns of the NiO-CoO hybrid and the $NiCo_2O_4$. As can be seen from Fig. 4a, the spacing between adjacent fringes is *ca.* 0.24 nm and 0.21 nm, close to the theoretical inter plane spacing of (111) and (200) planes of the NiO and CoO, respectively. the spacing between adjacent fringes in Fig. 4b is ca. 0.25nm and 0.2 nm, which are close to the theoretical inter plane spacing of (311) and (400) planes of the spinel $NiCo_2O_4$, respectively. Moreover, the selected-area electron diffraction (SAED) patterns in Fig. 4c and 4d separately show well-defined diffraction rings, suggesting their polycrystalline characteristics of the obtained NiO-CoO and $NiCo_2O_4$, which are in agreement with the XRD spectra in the Fig. 2a.

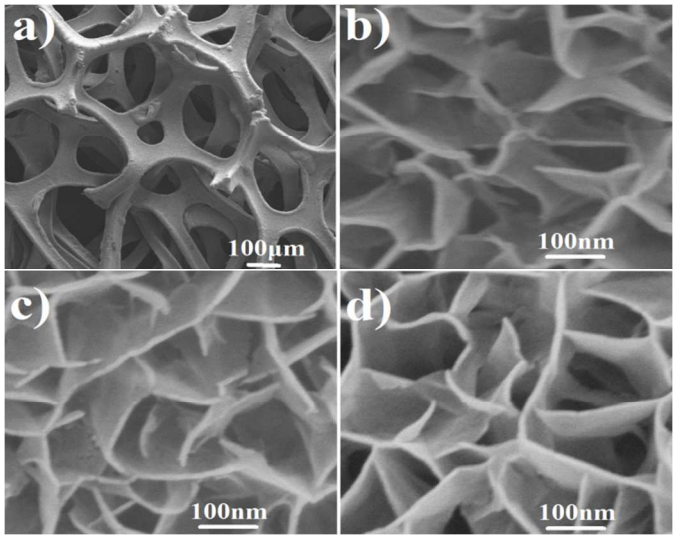

Fig. 3 SEM images of (a) nickel foam, (b) the Ni-Co LDH precursors, (c) the $NiCo_2O_4$, and (d) NiO-CoO hybrid.

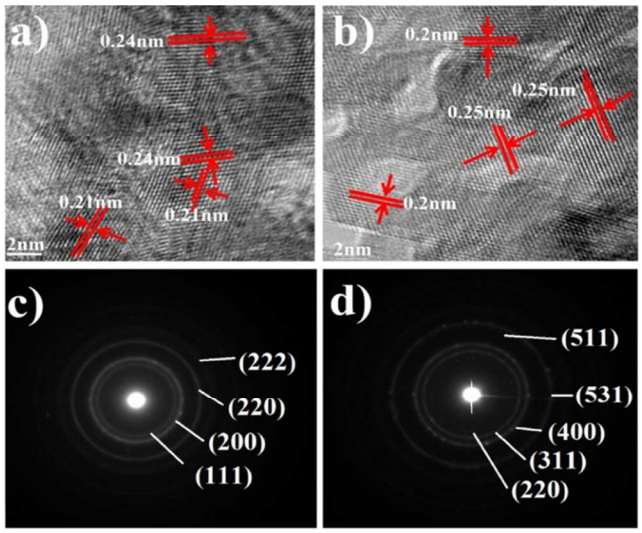

Fig. 4 HRTEM images, and SAED pattern of the NiO-CoO hybrid (a and c) and $NiCo_2O_4$ nanosheets (b and d) scratched down from the Ni foam.

Further TEM tests were carried out to investigate the beneficial morphology structure of the NiO-CoO hybrid electrode for supercapacitive application. As can be seen from Fig. 5a and b, the NiO-CoO hybrid nanosheets exhibit folding morphology with transparent feature, indicating the ultrathin nature. In addition, numerous inter-particle mesopores with a size ranged from 2 to 5 nm in these ultrathin nanosheets can be clearly seen (Fig. 5 a and b), which derives from the thermal decomposition of the hydroxides. It is well known that the mesoporous structures in nanosheets are important to facilitate the facile mass transport of electrolytes within the electrodes for fast redox reactions and double-layer charging/discharging. The porous structure will also greatly increase the electrode/electrolyte contact area, and thus further enhance the electrochemical performance. The Co/Ni molar rate was tested by an elemental mapping carried by the EDX-TEM in Fig. 5c-e. It is clear that the composition distributions of both Co and Ni are homogeneous throughout the nanosheets. Furthermore, the molar rate of Co/Ni is approximately 2, close to the Co/Ni molar rate in the stoichiometric $NiCo_2O_4$.

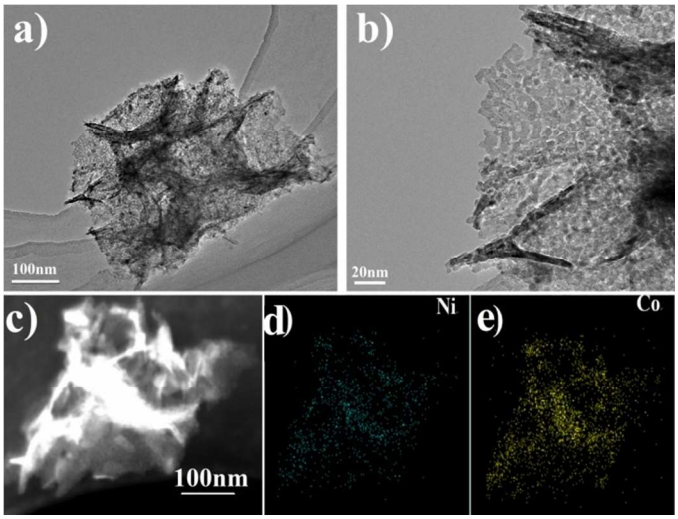

Figure 5. Characterization of the NiO-CoO hybrid sample: a,b) TEM images; c) TEM image for EDX-TEM mapping and elemental mapping of d) Ni and e) Co in c).

3.2 Electrochemical properties

Fig. 6 shows the cyclic voltammetry (CV) curves of the Ni@NiO-CoO hybrid electrode and the Ni@$NiCo_2O_4$ in the potential range of 0-0.55 V vs. Hg/HgO at a scan rate of 10 mV s^{-1} in 6M KOH aqueous electrolyte. It is clear that there are three pairs of peaks in the black curve, which indicates the strong pseudocapacitive nature of the obtained Ni@ NiO-CoO hybrid electrode. The first redox couple P1/P4 is due to the Co^{2+}/Co^{3+} reaction, while the second redox couple P2/P5 and the third redox couple P3/P6 are attributed to the Co^{3+} and Ni^{2+} converting to Co^{4+} and Ni^{3+}, respectively.[28-30, 42, 43] By comparison, there is only one broad redox couple P7/P8 for the Ni@$NiCo_2O_4$ electrode which is mainly related to the faradaic redox reactions related to M–O/M–O–OH, where M refers to Ni or Co.[44, 45] It is markedly that the Ni@NiO-CoO hybrid electrode containing multi-redox peaks demonstrated much stronger pseudocapacitive properties than the Ni@$NiCo_2O_4$ electrode, since the NiO-CoO hybrid containing Ni^{2+} and Co^{2+} ions shown much stronger pseudocapacitance between the Co^{2+}/Co^{3+} and Ni^{2+}/Ni^{3+} reaction than the $NiCo_2O_4$ mainly containing Co^{2+}, Co^{3+}, Ni^{2+} and Ni^{3+}.

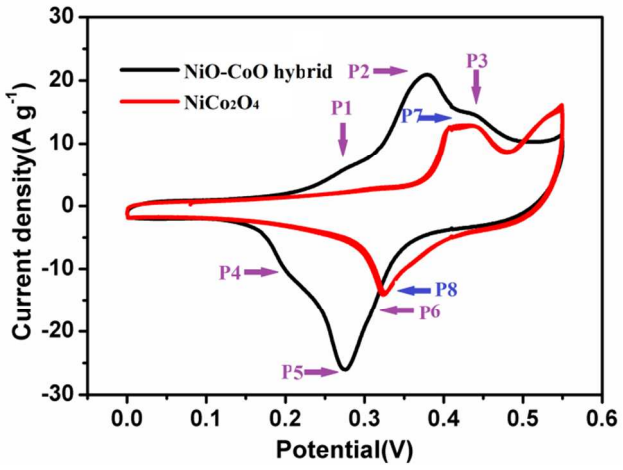

Fig. 6 CV curves of the he Ni@NiO-CoO hybrid electrode and the Ni@$NiCo_2O_4$ electrode at the same scanning rate.

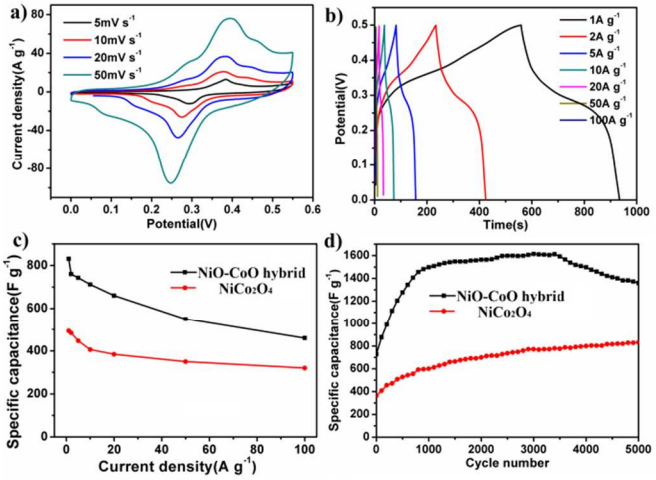

Fig. 7 (a) CV curves of the Ni@NiO-CoO hybrid electrode at different scanning rates, (b) GCD curves of the Ni@ NiO-CoO hybrid electrode at different current densities, (c) specific capacitance of the Ni@NiO-CoO hybrid electrode and the $NiCo_2O_4$ electrode at different current densities of 1, 2, 5, 10, 20, 50 and 100 A g^{-1}, (d) cycling performance of the Ni@ NiO-CoO hybrid electrode and the $NiCo_2O_4$ electrode at a current density of 10 A g^{-1}.

Fig. 7a shows the CV curves of the Ni@NiO-CoO hybrid electrode at different rates of 5, 10, 20 and 50 mV s^{-1}, which indicates the strong pseudocapacitance and excellent rate performance. Fig. 7b shows the galvanostatic charge and discharge curves of the Ni@NiO-CoO hybrid electrode with different current densities. There are obvious charge and discharge plateaus, characteristic of a typical pseudocapacitive behavior. The specific capacitance is calculated to be 831, 760, 743, 712, 660, 550 and 460 F g^{-1} at the current density of 1, 2, 5, 10, 20, 50, and 100 A g^{-1}, respectively. The capacitance retention rate is more than 53.5% when the current density was increased from 1 to 100 A g^{-1} that indicates the excellent rate performance of the prepared Ni@NiO-CoO hybrid electrode. The excellent electrochemical property of Ni@NiO-CoO hybrid can be associated with the synergistic effect of the advantageous nanostructure and the composition of the electrode. Firstly, the NiO-CoO hybrid obtained by annealing the Ni-Co LDHs in N_2 and H_2 gas entirely comprised of Ni^{2+} and Co^{2+} ions demonstrated strong pseudo-capacitance than the $NiCo_2O_4$. Secondly, high content of Co element (about twice than Ni element) entitled the electrode with high rate performance because CoO has better electronic conductivity than NiO. Thirdly , hydrogenolysis maybe enhance the electronic conductivity of the electrode and lead to enhanced electrochemical performance, since H_2 molecule is small enough to get into the electrode and hydrogenate the NiO and CoO. At last, the microstructure feature of the NiO-CoO hybrid containing meso- and micro- porous nanostructures is particularly advantageous to facilitate the electrolyte into the electrode quickly for redox reaction and double-layer charging–discharging.

Fig 7c shows the specific capacitances of Ni@$NiCo_2O_4$ and Ni@ NiO-CoO hybrid electrode as a function of current density. By comparison, we notice that the capacitance of Ni@NiO-CoO hybrid electrode is much higher than that of the Ni@$NiCo_2O_4$ at all different current densities. Cycling performance of the Ni@$NiCo_2O_4$ and Ni@NiO-CoO hybrid electrode are tested at the same current density of 10 A g^{-1} as shown in Fig. 7d. It can be observed that the specific capacitance of the Ni@NiO-CoO hybrid electrode increases obviously from 743 to 1500 F g^{-1} in the first 1000 cycles, and keeps increasing gradually up to the maximum of 1612 F g^{-1} in the 3400th

cycle, which can be attributed to the activation of the electrode. Afterwards, the specific capacitance begins to decline slowly, which is mainly due to the loss of active material and electrical contact caused by the mechanical stress between the NiO-CoO nanostructure and the nickel foam.[44, 46] After 5000 cycles, the capacitance of the hybrid electrode still remained a value of 1360 F g^{-1} which is 84.4% of the peak value, 191% of the pristine value. By comparison, the $NiCo_2O_4$ electrode has much better cycle life than NiO-CoO because the spinel $NiCo_2O_4$ has better electronic conductivity than the unitary NiO and CoO. However, an increasing specific capacitance up to the maximum of 830 F g^{-1} after 5000 cycles which is still lower than that of the Ni@NiO-CoO hybrid electrode. The good electrochemical properties with a high specific capacitance and long cycling stability shows that the Ni@ NiO-CoO hybrid electrode is very promising electrode materials for the next generational supercapacitors.

To explain the excellent electrochemical performance of the Ni@NiO-CoO hybrid electrode better, impedance spectra of the Ni@NiO-CoO hybrid electrode and the Ni@$NiCo_2O_4$ electrode before the cycling texts were texted and shown in Fig. 8a. Each of the impedance spectra includes a sloped line in the low-frequency and one semicircle in the high frequency. Fig. 8a shows the impedance spectra of the Ni@NiO-CoO hybrid electrode and the before the cycling texts. As shown in Fig. 8a, in the high frequency area, the solution resistance (Rs) of the Ni@NiO-CoO hybrid electrode was only 0.42 Ω which is lower than 0.47Ω for the Ni@$NiCo_2O_4$ electrode at the high frequency intercept of the real axis. In addition, the diffusive resistance (Warburg impedance) of Ni@NiO-CoO hybrid electrode was also lower than the Ni@$NiCo_2O_4$ electrode in lower frequencies. The ultimate results indicate that the electron conductivity of Ni@NiO-CoO hybrid electrode is much better than the Ni@$NiCo_2O_4$ electrode. In fig. 8b, the solution resistance (Rs) of the Ni@NiO-CoO hybrid electrode after 5000 cycles increased from 0.42 Ω to 0.841Ω and the diffusive resistance was also higher than the fresh electrode. These results may be because of the surface and microstructural changes of the Ni@NiO-CoO hybrid electrode after 5000 cycles. As a result, the specific capacitance of Ni@NiO-CoO hybrid electrode declined gradually. SEM image of the Ni@NiO-CoO hybrid electrode after 5000 cycles was presented in Fig. 9. It is clear that the surface morphology of the Ni@NiO-CoO hybrid nanosheet electrode was slightly changed and different from the intact nanosheets before cycling as shown in Fig. 3 (d). It can be deduced that the Ni@NiO-CoO hybrid nanosheets peeled off partly from the nickel form current collectors which led to gradually decreasing specific capacitance of the Ni@NiO-CoO hybrid electrode after long cycling.

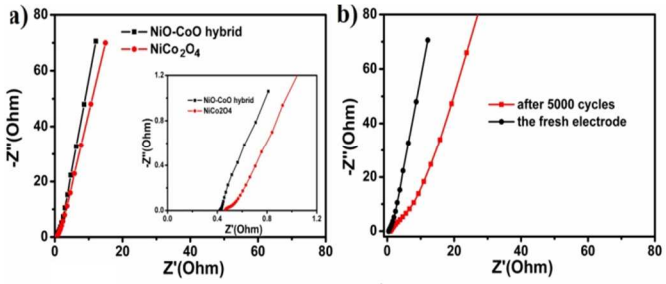

Fig. 8 (a) Nyquist curve of the Ni@NiO-CoO hybrid electrode and the $NiCo_2O_4$ electrode before cycling, (b) Nyquist curves of the Ni@NiO-CoO hybrid electrode before and after 5000 cycling.

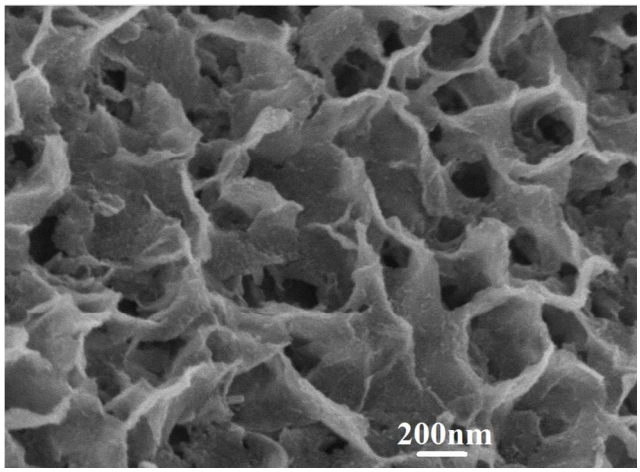

Fig. 9 SEM image of NiO-CoO hybrid after 5000 cycles.

4. Conclusions

In summary, a novel NiO-CoO nanosheets hybrid directly grown on nickel foam was synthesized by electro-deposition and annealed in the 5% H_2/95% N_2 mixed gas. The hydrogenated Ni@ NiO-CoO hybrid electrode evaluated for supercapacitors exhibited much enhanced electrochemical properties than the traditional Ni@$NiCo_2O_4$ electrode. The Ni@ NiO-CoO hybrid electrode showed the highest specific capacitance of 1612 F g^{-1} and high retention of 1360 F g^{-1} at the current of 10 A g^{-1} after 5000 cycles.

Acknowledgements

This work was supported by the Shenzhen Peacock Plan (KQCX20140522150815065), the Starting-Up Funds of South University of Science and Technology of China (SUSTC) through the talent plan of the Shenzhen Government, and the National Natural Science Foundation of China (21001117).

Notes and references

[a] School of Chemistry & Chemical Engineering, Central South University, Changsha, Hunan 410083, China. E-mail: guyy02@163.com (GYY)
[b] Department of Materials Science and Engineering, South University of Science and Technology of China, Shenzhen, Guangdong 518055, China. E-mail: luzg@sustc.edu.cn (LZG)

1. Y. Fu, X. Cai, H. Wu, Z. Lv, S. Hou, M. Peng, X. Yu and D. Zou, *Advanced Materials*, 2012, **24**, 5713-5718.
2. G. Wang, L. Zhang and J. Zhang, *Chemical Society Reviews*, 2012, **41**, 797-828.
3. P. Simon and Y. Gogotsi, *Nature materials*, 2008, **7**, 845-854.
4. J. R. Miller and P. Simon, *Science Magazine*, 2008, **321**, 651-652.
5. H. Xia, Y. S. Meng, G. Yuan, C. Cui and L. Lu, *Electrochemical and Solid-State Letters*, 2012, **15**, A60-A63.
6. N. Nagarajan, H. Humadi and I. Zhitomirsky, *Electrochimica Acta*, 2006, **51**, 3039-3045.
7. F. Li, J. Song, H. Yang, S. Gan, Q. Zhang, D. Han, A. Ivaska and L. Niu, *Nanotechnology*, 2009, **20**, 455602.
8. Z. Chen, V. Augustyn, J. Wen, Y. Zhang, M. Shen, B. Dunn and Y. Lu, *Advanced Materials*, 2011, **23**, 791-795.
9. X. Zhu, Y. Zhu, S. Murali, M. D. Stoller and R. S. Ruoff, *Acs Nano*, 2011, **5**, 3333-3338.
10. J. Mu, B. Chen, Z. Guo, M. Zhang, Z. Zhang, P. Zhang, C. Shao and Y. Liu, *Nanoscale*, 2011, **3**, 5034-5040.
11. J.-W. Lang, L.-B. Kong, W.-J. Wu, Y.-C. Luo and L. Kang, *Chemical Communications*, 2008, 4213-4215.
12. X.-h. Xia, J.-p. Tu, Y.-j. Mai, X.-l. Wang, C.-d. Gu and X.-b. Zhao, *Journal of Materials Chemistry*, 2011, **21**, 9319-9325.

13. C. Zhou, Y. Zhang, Y. Li and J. Liu, *Nano letters*, 2013, **13**, 2078-2085.
14. G. Q. Zhang, H. B. Wu, H. E. Hoster, M. B. Chan-Park and X. W. D. Lou, *Energy & Environmental Science*, 2012, **5**, 9453-9456.
15. C. Yuan, J. Li, L. Hou, X. Zhang, L. Shen and X. W. D. Lou, *Advanced Functional Materials*, 2012, **22**, 4592-4597.
16. G. Zhang and X. W. D. Lou, *Scientific reports*, 2013, **3**.
17. Y. Yuan, H. Bi, G. He, J. Zhu and H. Chen, *Chemistry Letters*, 2014, **43**, 83-85.
18. S. Jiang, T. Shi, H. Long, Y. Sun, W. Zhou and Z. Tang, *Nanoscale research letters*, 2014, **9**, 1-8.
19. Y. Xu, X. Wang, C. An, Y. Wang, L. Jiao and H. Yuan, *Journal of Materials Chemistry A*, 2014, **2**, 16480-16488.
20. K. Karthikeyan, D. Kalpana and N. Renganathan, *Ionics*, 2009, **15**, 107-110.
21. B. Liu, B. Liu, Q. Wang, X. Wang, Q. Xiang, D. Chen and G. Shen, *ACS applied materials & interfaces*, 2014, **6**, 2199-2199.
22. S. Peng, L. Li, H. B. Wu, S. Madhavi and X. W. D. Lou, *Advanced Energy Materials*, 2014.
23. D. Guo, Y. Luo, X. Yu, Q. Li and T. Wang, *Nano Energy*, 2014, **8**, 174-182.
24. D. Guo, H. Zhang, X. Yu, M. Zhang, P. Zhang, Q. Li and T. Wang, *Journal of Materials Chemistry A*, 2013, **1**, 7247-7254.
25. X. Yu, B. Lu and Z. Xu, *Advanced Materials*, 2014, **26**, 1044-1051.
26. J. Liu, J. Jiang, C. Cheng, H. Li, J. Zhang, H. Gong and H. J. Fan, *Advanced Materials*, 2011, **23**, 2076-2081.
27. L.-Q. Mai, F. Yang, Y.-L. Zhao, X. Xu, L. Xu and Y.-Z. Luo, *Nature communications*, 2011, **2**, 381.
28. X. Xia, J. Tu, Y. Zhang, X. Wang, C. Gu, X.-b. Zhao and H. J. Fan, *ACS nano*, 2012, **6**, 5531-5538.
29. C. Guan, X. Li, Z. Wang, X. Cao, C. Soci, H. Zhang and H. J. Fan, *Advanced Materials*, 2012, **24**, 4186-4190.
30. J.-H. Zhong, A.-L. Wang, G.-R. Li, J.-W. Wang, Y.-N. Ou and Y.-X. Tong, *Journal of Materials Chemistry*, 2012, **22**, 5656-5665.
31. V. Gupta, S. Gupta and N. Miura, *Journal of Power Sources*, 2008, **175**, 680-685.
32. S. Li, Y. Liu, Y. Liu and Y. Chen, *Journal of Power Sources*, 2010, **195**, 7202-7206.
33. J. W. Lee, T. Ahn, J. H. Kim, J. M. Ko and J.-D. Kim, *Electrochimica Acta*, 2011, **56**, 4849-4857.
34. C. Yuan, X. Zhang, L. Su, B. Gao and L. Shen, *Journal of Materials Chemistry*, 2009, **19**, 5772-5777.
35. S.-I. Kim, J.-S. Lee, H.-J. Ahn, H.-K. Song and J.-H. Jang, *ACS applied materials & interfaces*, 2013, **5**, 1596-1603.
36. B. Cui, H. Lin, Y.-z. Liu, J.-b. Li, P. Sun, X.-c. Zhao and C.-j. Liu, *The Journal of Physical Chemistry C*, 2009, **113**, 14083-14087.
37. M. P. Seah and D. Briggs, *Practical Surface Analysis: Auger and X-ray Photoelectron Spectroscopy*, John Wiley & Sons, 1990.
38. V. Jimenez, A. Fernandez, J. Espinos and A. Gonzalez-Elipe, *Journal of Electron Spectroscopy and Related Phenomena*, 1995, **71**, 61-71.
39. B. Marcus-Saubat, J. Beaufils and Y. Barbaux, *Journal de chimie physique*, 1986, **83**, 317-321.
40. T. Chuang, C. Brundle and D. Rice, *Surface Science*, 1976, **59**, 413-429.
41. J.-G. Kim, D. Pugmire, D. Battaglia and M. Langell, *Applied surface science*, 2000, **165**, 70-84.
42. W. Chen, C. Xia and H. N. Alshareef, *ACS nano*, 2014, **8**, 9531-9541.
43. L. Cao, F. Xu, Y. Y. Liang and H. L. Li, *Advanced materials*, 2004, **16**, 1853-1857.
44. Z. Wang, Y. Zhang, Y. Li and H. Fu, *RSC Advances*, 2014, **4**, 20234-20238.
45. G. Q. Zhang, H. B. Wu, H. E. Hoster, M. B. Chan-Park and X. W. Lou, *Energy & Environmental Science*, 2012, **5**, 9453-9456.
46. R. Wang, Z. Chen, H. Yu, X. Jia, L. Gao, J. Sun, R. F. Hicks and Y. Lu, *Nanoscale*, 2014, **6**, 3791-3795.

Three-dimensional bind-free NiO-CoO hybrid electrodes were directly grown on the nickel foam by electrodeposition and hydrogenolysis in 5% H_2/ 95% N_2 gas. The hydrogenated NiO-CoO hybrid electrodes shown much better electrochemical performance for supercapacitors than the Ni@ $NiCo_2O_4$ electrodes obtained by annealing in pure N_2 gas.